Origin and designing of large ground-state zero-field splitting of color centers in diamond

Chen Qiu,[1] Han-Pu Liang,[1] Hui-Xiong Deng,[2] and Su-Huai Wei[1,*]

[1]*Beijing Computational Science Research Center, Beijing 100094, China*

[2]*State Key Laboratory of Superlattices and Microstructures, Institute of Semiconductors, Chinese Academy of Sciences & Center of Materials Science and Optoelectronics Engineering, University of Chinese Academy of Sciences, Beijing 100083, China*

(Received 20 February 2024; revised 8 June 2024; accepted 24 June 2024; published 8 July 2024)

In diamond, the pivotal factor for quantum applications involving color centers hinges on extending the spin coherence time through a larger ground-state zero-field splitting (ZFS). Experimental observations indicate a correlation between the atomic number and the increasing of the ground-state ZFS of group-IV centers. Yet, the physical origin underlying the impurity-modulated ground-state ZFS remains insufficiently elucidated. In this study, utilizing density-functional theory and group analysis, we illustrate that the origin of the correlation between the ground-state ZFS in group-IV centers and the atomic number of impurity atoms, arises from the synergistic interplay of large atomic numbers and the extent of *p-d* orbital hybridization. Simultaneously, our investigation identifies that the ground-state of group-IVB centers originates from a robust *p-p* hybridization between impurity atom and divacancy. This interaction results in ground-state ZFS of 7728 GHz for HfV^- centers, nearly doubling the experimentally observed value found in the largest PbV^- centers. Our study, therefore, provides profound insights into the origins of the impurity-modulated ground-state ZFS, offering a promising pathway towards achieving larger ground-state ZFS of color centers.

DOI: 10.1103/PhysRevB.110.024104

I. INTRODUCTION

Point defect-related color centers in diamonds show great promise for applications in quantum computers, quantum communication, and quantum networks [1–6]. The negatively charged nitrogen-vacancy (NV^-) color center, among the various color centers in diamond, has been the subject of intense study. This is primarily because its spin state exhibits long spin coherence time (T_2) that is not limited by spin-lattice interaction [7,8], and can be optically initialized, manipulated, and read out at room temperature [9–11]. However, despite these favorable characteristics, the coherence optical emission at the zero-phonon line of the NV center is only 3% of its total fluorescence, even at cryogenic temperature. This limitation is attributed to the substantial spectral diffusion and phonon sideband, resulting in reduced coherent photon generation rates and optical transition instability [12–15]. These challenges severely impede the development of the NV center for quantum applications. Recent investigations indicate that the group-IV-vacancy color centers exhibit inversion symmetry (D_{3d} point group) because the impurity atoms (Si, Ge, Sn, Pb) have relatively large sizes, therefore they autonomously depart from the substitution position to create split-vacancy configurations, leading to resistance to external noise and negligible spectral diffusion [16–20]. This unique behavior results in robust zero-phonon line (ZPL) emission and constitutes 60–70% of the total spectrum for the group-IV color centers, showcasing the potential to overcome the disadvantages found in the NV center [21–23].

The pivotal factor for implementing quantum applications of group-IV centers is the spin coherence time T_2, which faces limitations due to orbital relaxation arising from single-phonon processes [18,22,24,25]. Ensuring $k_BT \ll h\Delta_{GS}$ can reduce the phonon absorption in the ground-state manifold, given that the phonon-mediated transition rate is proportional to the occupation of the phonon mode, denoted as $n(T, \Delta_{GS}) = 1/(e^{h\Delta_{GS}/k_BT} - 1)$, where Δ_{GS} signifies the ground-state zero-field splitting (ZFS) arising from the spin-orbit coupling (SOC) effect. Here, h represents the Planck constants, T denotes temperature, and k_B stands for Boltzmann constants. Consequently, two strategies can enhance the spin coherence time of color centers with inversion symmetry. One approach involves cooling the sample to $k_BT \ll h\Delta_{GS}$, exemplified by the SiV^- center with Δ_{GS} equal to 50 GHz [26–28]. While the spin coherence time at 4 K is only 45 ns, it extends to 13 ms at 100 mK [16,29]. However, the substantial decrease in operating temperatures imposes limitations on the quantum applications of the color center. Another possible avenue to achieve a prolonged spin coherence time at higher temperature is to explore the novel color center with a large Δ_{GS} [30–33]. For instance, the SnV^- center with Δ_{GS} of 850 GHz achieves a spin coherence time of 0.3 ms at 1.7 K [18,34]. The PbV^- center has Δ_{GS} of 4227 GHz ($\sim$ 17.5 meV), thus it is anticipated that the PbV^- center operated at 9 K can exhibit the same spin coherence time as the SiV^- center at 0.4 K or the SnV^- center at 2 K [23,35]. Hence, the design for color centers with substantial Δ_{GS} can effectively enhance spin coherence time and operational temperatures. The observed increasing trend in Δ_{GS} with atomic

*Present address: Eastern Institute of Technology, Ningbo 315200, China; Contact author: suhuaiwei@eitech.edu.cn

number among group-IV color centers, particularly the large Δ_{GS} of PbV^- centers reaching terahertz frequencies, is generally attributed to the heavy atomic mass and large atomic number of Pb [19,25]. However, prior studies indicate that the primary contribution to the ground-state Γ_3^+ (e_g) state of group-IV color centers mainly arises from dangling bonds associated with divacancies, especially in the case of the SiV^- center, where the ground-state Γ_3^+ (e_g) state is entirely composed of dangling bonds from divacancies [20,36]. Therefore, a more profound understanding of the physical origin of the modulation of Δ_{GS} by impurity atoms is a prerequisite for designing color centers with larger Δ_{GS}.

In this study, we comprehensively investigated the ground-state ZFS of color centers in diamond involving group-III (In, Tl), group-IV (Si, Ge, Sn, Pb), group-V (Sb, Bi), and group-IVB (Ti, Zr, Hf) color centers. Our findings elucidate several key observations: (i) The progressive increase in ground-state ZFS within group-IV centers correlates with the atomic number of impurity atoms, attributed to the synergistic interplay between large atomic numbers and the extent of *p-d* orbital hybridization. (ii) Enhanced *p-d* coupling originating from the higher *d* orbital of group-III impurities results in a large ground-state ZFS of 5637 GHz for the TlV^{2-} center, surpassing the experimentally observed 4227 GHz of PbV^- centers. (iii) The ground state of group-IVB centers is established from a robust *p-p* hybridization. This hybridization incorporates a substantial portion of the *p* orbital components of the group-IVB atom, leading to a ground-state ZFS of 7728 GHz for HfV^- centers, nearly double the experimentally observed value in the largest PbV^- centers. Consequently, our study unveils the underlying physical mechanisms governing the modulation of ground-state ZFS by impurity atoms. This understanding paves the way for the design of color centers characterized by large ground-state ZFS, thereby presenting a promising avenue for achieving prolonged spin coherence times at elevated temperatures.

II. COMPUTATIONAL METHOD AND FORMULATION

Our band structure and total energy calculations employed spin-polarized density function theory (DFT) as implemented in the VASP.6.2.1 package, utilizing the Perdew-Burke-Ernzerhof (PBE) exchange-correlation functional [37,38]. A 400-eV energy cutoff was applied for the plane-wave expansion within the projector-augmentation wave method (PAW) [39]. We adopted a 1000-atom supercell to explore color centers in diamond, encompassing group-III (In, Tl), group-IV (Si, Ge, Sn, Pb), group-V (Sb, Bi), and group-IVB (Ti, Zr, Hf) color centers. This 1000-atom supercell guarantees a converged charged density by sampling the Brillouin zone at the Γ point, and effectively avoiding the Coulomb interaction between the periodic cells [25]. All atomic positions undergo relaxation until forces on individual atoms reaches below 10^{-4} eV/Å. To ensure precision in electronic band structures and total energies, we incorporated the Heyd-Scuseria-Ernzerhf (HSE06) hybrid functional method with a mixing parameter of 0.28 [40,41]. The indirect band gap calculated using HSE06 is 5.44 eV, aligning closely with the previously reported experimental value of 5.48 eV [42].

To evaluate the ZFS, which is the splitting of the highest occupied doubly degenerate state in the gap (see Fig. 1) caused by the spin-orbit coupling (SOC), we employ the SOC Hamiltonian in the band structure calculations with [43]

$$\hat{H}_{SOC} = \frac{\hbar}{(2Mc)^2}\frac{1}{r}\frac{dV}{dr}\hat{L}\cdot\hat{S},$$
$$M = m + \frac{\epsilon - V}{2c^2}, \quad (1)$$

where M is the enhanced relativistic electron mass, c is the speed of light, V is the effective potential, ϵ is the eigenvalue, and $\hat{L}$ is the effective orbital moment operator of the electron, while $\hat{S}$ is the electronic spin.

III. RESULTS AND DISCUSSION

In the pursuit of understanding the impurity-induced modification in ground-state ZFS (Δ_{GS}) due to spin-orbit coupling, as shown in Table I, we first calculated the Δ_{GS} of various color centers in diamond. Considering the advantageous characteristics of a negatively single charged group-IV color center, all color centers analyzed in this study maintain an equivalent number of electrons, encompassing group-III (InV^{2-}, TlV^{2-}), group-IV (SiV^-, GeV^-, SnV^- and PbV^-), group-V (SbV^0, BiV^0) and group-IVB (TiV^-, ZrV^-, HfV^-) color centers. The direct calculation from Kohn-Sham orbitals revealed intrinsic ground-state ZFS (Δ_{GS}^0), i.e., the level splitting of ground state Γ_3^+ in Fig. 1 for SiV^- and XV (X = Ge, Sn, Pb, In, Tl, Sb, Bi) centers or Γ_3^- in Fig. 3 for MV^- (M = Ti, Zr, Hf). As presented in Table I, in color centers featuring impurity atoms from identical groups, a general trend is that the Δ_{GS} rapidly grows with the atomic number. Yet, among color centers featuring impurities within the same period, the Δ_{GS} showcases an opposite trend, decreasing with the increase of atomic number. The observed rise in Δ_{GS} of group-IV color centers is currently predominantly attributed to the increasing atomic number, thus, spin-orbit coupling of the impurities. However, this explanation stands in contrast to the observed reduction in Δ_{GS} for color centers with impurities in the same period. Indeed, a profound understanding of the fundamental origins of Δ_{GS} of color centers in diamond has been conspicuously absent. We will elucidate these general trends based on group theory and band coupling mechanisms.

First, the band-coupling mechanism is employed to unveil the underlying physical origins of the pronounced increase in Δ_{GS} corresponding to the atomic number variations among the same group. The mechanism delineates defect states arising from coupling between the divacancy dangling bond states and impurity atomic orbitals, as illustrated in Fig. 1. Within split-vacancy configurations featured in a local D_{3d} crystal field, the divacancy leaves six C dangling bonds around the impurity atom. These bonds interact to form a_{1g}, a_{2u}, e_g, and e_u states, while the four sp^3 orbitals of impurity contribute a_{1g}, a_{2u}, and e_u states [20,36]. Consequently, the a_{1g}, a_{2u}, and e_u states of divacancy and impurity combine to create occupied Γ_1^+, Γ_2^-, and Γ_3^- bonding states and the Γ_3^+ state within the band gap. The Γ_3^+ state comprises almost solely C dangling bond states for SiV^- center without valence d orbitals. On the other hand, the doubly degenerate $d_{x^2-y^2} + d_{xy}$ and $d_{xz} + d_{yz}$

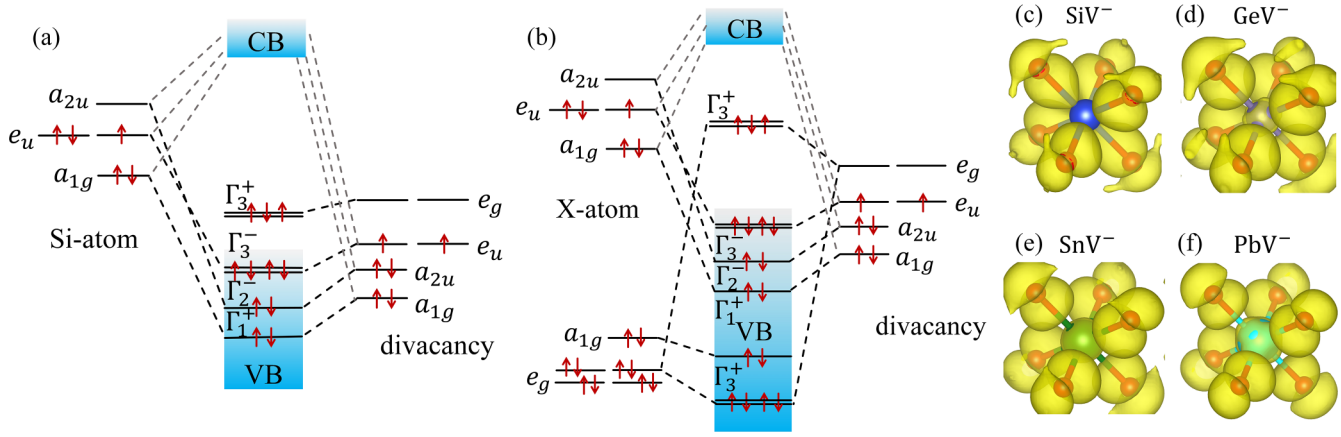

FIG. 1. Band-coupling diagrams depicting for (a) SiV^- without valence d orbital and (b) XV (X = Ge, Sn, Pb, In, Tl, Sb, Bi) with d orbital centers in diamond. All impurity color centers consider the same number of defect electrons as the negatively charged group-IV centers. The irreducible representations of atomic orbitals and defect states under the D_{3d} point group are presented. Specifically, the coupling of orbitals between X atoms and six-carbon dangling-bond states of the divacancy in diamond are illustrated, forming the defect states as illustrated. Notably, for the sake of simplicity, the diagrams do not consider level splitting induced by spin-orbit coupling. The local relaxed geometry and three-dimensional partial charge density (yellow: isosurface of 0.002 e^-/bohr^3) for Γ_3^+ state of (c) SiV^-, (d) GeV^-, (e) SnV^-, and (f) PbV^- color center in a diamond supercell along (0 0 1) direction. The red-colored balls represent host carbon atoms, and the blue, purple, green, and cyan balls denote silicon, germanium, tin, and lead atoms, respectively.

orbitals of X (X = Ge, Sn, Pb, In, Tl, Sb, Bi) atoms, characterized by the irreducible representation e_g, couple with the e_g state of divacancy and thus contribute significantly to the formation of the antibonding state Γ_3^+ within the band gap for XV centers. This can be seen in Figs. 1(c)–1(f), where the three-dimensional partial charge distribution of SiV^- showcases the Γ_3^+ state consisting entirely of the C dangling bonds, while the Γ_3^+ state of XV centers primarily comprises the C dangling bond states and partially includes impurity d orbitals.

The coupling strength between the two p and d orbitals is proportional to $V_{pd}^2 = |\langle p|\Delta V|d\rangle|^2$ and $1/|\varepsilon_p - \varepsilon_d|\, d^2$, where ΔV is the coupling potential, $|\varepsilon_p - \varepsilon_d|$ is the energy level difference, and d represents the bond length [44,45]. The energy associated with the d orbitals of group-IV atoms are shown in Table II, increases with the atomic number, i.e., −29.22 eV for the Ge atom, −25.77 eV for the Sn atom, and 21.12 eV for the Pb atom. This results in a stronger p-d orbital coupling between the divacancy and the impurity atom, leading to higher Γ_3^+ state energy. Indeed, as depicted in Fig. 2, the single-particle levels, determined using the HSE06 method, exhibit an upward trend from SiV^- to PbV^-, namely 1.81 eV for *the* SiV^- center, 2.33 eV for *the* GeV^- center, 2.65 eV for the SnV^- center, and 3.12 eV for the PbV^- center. Hence,

TABLE I. The computed parameters related to obtain the effective spin-orbit coupling Δ_{GS}^{Ham}. These include the Jahn-Teller stabilization energy E_{JT}, the effective e_g and e_u phonon energy $\hbar\omega$ that drives the Jahn-Teller effect, the calculated intrinsic spin-orbit coupling Δ_{GS}^0, the Ham reduction factor p, and the derived effective spin-orbit coupling $\Delta_{GS}^{Ham} = p\Delta_{GS}^0$. The calculated Δ_{GS}^{Ham} is compared to the available experimental data Δ_{GS}^{expt}.

System	Δ_{GS}^0 (meV, GHz)	E_{JT} (meV)	$\hbar\omega$ (meV)	p	Δ_{GS}^{Ham} (GHz)	Δ_{GS}^{expt}(GHz)
SiV^-	0.97, 234	43.05	89.59	0.36	84	50[a]
GeV^-	2.21, 534	30.87	84.50	0.43	230	184[b]
SnV^-	7.77, 1877	22.06	85.15	0.52	976	850[c]
PbV^-	31.73, 7664	15.17	73.17	0.58	4445	4227[d]
InV^{2-}	11.67, 2818	17.13	69.51	0.54	1522	
TlV^{2-}	44.88, 10 841	18.96	70.60	0.52	5637	
SbV^0	5.96, 1440	30.19	91.15	0.46	662	
BiV^0	21.73, 5249	20.41	88.83	0.56	2939	
TiV^-	16.24, 3923	49.09	58.73	0.21	824	
ZrV^-	49.85, 12 041	46.94	58.66	0.22	2649	
HfV^-	168.38, 40 671	47.91	53.44	0.19	7728	

[a]Reference [27].
[b]Reference [30].
[c]Reference [18].
[d]Reference [23].

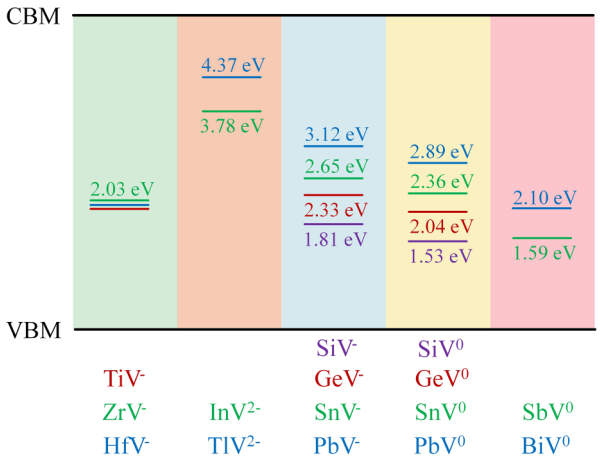

FIG. 2. The single-particle levels of color centers in diamond are determined using the HSE06 method. Color centers introduced by elements within the same period and their corresponding single-particle levels are depicted using identical colors scheme. The single-particle levels correspond to the Γ_3^+ state in Fig. 1 or the Γ_3^- state in Fig. 3 (i.e., the highest defect energy level occupied by electrons).

the rapid increase observed in the Δ_{GS} from SiV^- to GeV^-, SnV^-, and PbV^- centers stem from the synergistic interplay between the large SOC of a heavy atom and the extent of *p-d* orbital hybridization, as reflected by the calculated intrinsic ground-state ZFS of 234 GHz for SiV^- centers, 534 GHz for GeV^- centers, 1877 GHz for SnV^- centers, and 7664 GHz for PbV^- centers, as presented in Table I. Notably, these results closely align with previous DFT calculations [19,25].

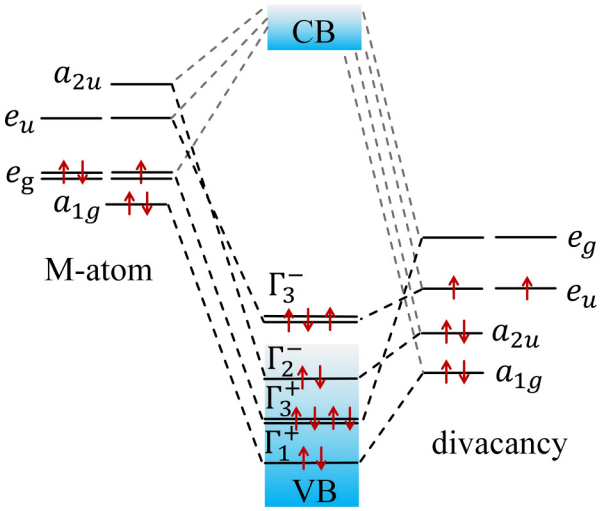

FIG. 3. Band-coupling diagrams depicting for MV^- (M = Ti, Zr, Hf) centers in diamond. The irreducible representations of atomic orbitals and defect states under the D_{3d} point group are presented. Specifically, the coupling of orbitals between M atoms and six-carbon dangling-bond states of the divacancy in diamond are illustrated, forming the defect states as outlined schematically. Notably, for the sake of simplicity, the diagrams do not consider level splitting induced by spin-orbit coupling, and some uninvolved empty orbitals have been omitted.

TABLE II. The valence *s*, *p*, and *d* orbital-energy levels (in eV) of group-III (In, Tl), group-IV (Si, Ge, Sn, Pb), group-V (Sb, Bi), and group-IVB (Ti, Zr, Hf) atoms, respectively.

Atom	Eigenvalue (ns)	Eigenvalue (np)	Eigenvalue ($n-1$) d
C	−13.64	−5.42	
Si	−10.74	−4.01	
Ge	−11.66	−3.82	−29.22
Sn	−10.41	−3.59	−25.77
Pb	−11.87	−3.39	−21.12
In	−8.11	−2.42	−18.51
Tl	−9.44	−2.27	−15.38
Sb	−12.74	−4.74	−33.40
Bi	−14.36	−4.45	−26.95
Ti	−4.46	−1.54	−4.46
Zr	−4.59	−1.55	−3.74
Hf	−5.27	−1.47	−2.87

However, they starkly contrast with experimentally reported Δ_{GS}^{expt} results: 50 GHz for SiV^- centers, 184 GHz for GeV^- centers, 850 GHz for SnV^- centers, and 4227 GHz for PbV^- centers [18,23,27,30]. This discrepancy can be attributed to the dynamic Jahn-Teller (DJT) effect, which quenches the orbital moment, a phenomenon known as the Ham effect [25,46–48]. Within DJT systems, the DJT effect effectively reduces the strength of the SOC by a reduction factor p denoted as the Ham reduction factor (see the Appendix), i.e., $\Delta_{GS}^{Ham} = p\Delta_{GS}^{0}$. This reduction consequently diminishes the magnitude of the intrinsic Δ_{GS}^{0}, aligning more closely with experimentally reported Δ_{GS}^{expt} values.

The Pb atom stands among the heaviest group-IV elements in the periodic table of elements, which restricts the design of the color center with larger Δ_{GS} by merely seeking even heavier elements. It is foreseeable that higher energy levels of d orbitals within the impurity atom could engender stronger *p-d* orbital coupling, potentially offering a pathway for developing a color center with amplified Δ_{GS}. This is confirmed by our computed Δ_{GS}^{Ham} for group-III and group-V color centers: 1522 GHz for InV^{2-} centers, 5637 GHz for TlV^{2-} centers, 662 GHz for SbV^0 centers, and 2939 GHz for BiV^0 centers, that is a progressive decrease in the Δ_{GS} of XV centers from group-III to group-IV to group-V centers, despite sharing similar electronic structures and with increasing atomic numbers. This is because the d orbital energies of elements within the same period display a notable deepening from group-III to group-IV to group-V elements (see Table II). For instance, the d orbital energy levels for In, Sn, and Sb atoms are −18.51, −25.77, and −33.40 eV, respectively. This deepening of the d orbital energy results in a weakened *p-d* coupling between the impurity atom and divacancy, leading to the observed attenuation in Δ_{GS}^{Ham} from InV^{2-} centers to SnV^- to SbV^0 centers. This gradual weakening of the *p-d* coupling is further illustrated in Fig. 2, which illustrates the diminishing trend in *p-d* coupling and thus the single-particle levels of group-III, group-IV, and group-V centers. As a consequence of strong *p-d* coupling, the Δ_{GS} of TlV^{2-} centers at 5637 GHz surpass that observed experimentally in PbV^- centers, despite the Tl atom having a smaller atomic number than the Pb atom.

With the above understanding, one can anticipate that transition metal elements, characterized by their high d orbital energies, may have the potential to introduce color centers in diamond with larger Δ_{GS} compared to group-III, group-IV, and group-V color centers. Indeed, TiV^-, ZrV^-, and HfV^- centers exhibit larger Δ_{GS}^{Ham}, specifically 824 GHz for TiV^-, 2649 GHz for ZrV^-, and 7728 GHz for HfV^- centers. However, these larger Δ_{GS}^{Ham} of MV^- (M = Ti, Zr, Hf) centers do not stem from stronger p-d orbital coupling. This distinction from the XV centers arises from the fact that, in comparison to the d orbitals of X atoms, the valence d orbitals of M atoms possess higher energies than p orbital of C atoms, as shown in Table II. Consequently, this scenario results in a robust p-d orbital coupling, making the bonding state Γ_3^+ to be lower in energy than the bonding state Γ_3^- and the positioning Γ_3^+ state falls below the valence band maximum (VBM). As illustrated in Fig. 3, the gap state of MV^- centers are the Γ_3^- state, representing the bonding state between the e_u orbital of divacancy and the e_u orbital of the M atom. Because the inherently more delocalized nature of p orbitals and the small energy difference between the e_u orbital of the M atom and the e_u orbital of divacancy, the bonding state Γ_3^-, due to the p-p orbital hybridization, incorporates a greater portion of the M atom's p orbital components, resulting in a Δ_{GS}^{Ham} far exceeding that of XV centers. Thus, the Δ_{GS} of HfV^- centers are nearly twice that observed experimentally in the largest PbV^- centers. Utilizing the formula $T = h\Delta_{GS}/k_b$ for estimating the up limit of the temperature at which the system can work at with good coherence [32], we find that the temperature T is approximately 370 K for the HfV^- center, showcasing the potential to achieve extended spin coherence time, particularly at elevated temperatures.

Finally, as depicted in Fig. 1, the ground and excited state of XV centers correspond to the Γ_3^+ and Γ_3^- state, respectively. However, as shown in Fig. 3, the presence of strong p-d coupling in HfV^- centers leads to a lower energy for the Γ_3^+ state. Consequently, the ground state and excited state are identified as the Γ_3^- and Γ_3^+ state, respectively. Both group-IV centers and HfV^- centers exhibit optical pumping and nonradiative transitions between the Γ_3^+ and Γ_3^- states. The only difference lies in the relative positions of the ground and excited states. Hence, the optical characteristics governing initialization and readout are expected to remain similar across these color centers. The calculated transition dipole moments from ground state to excited state for PbV^- and HfV^- centers are 34.4 and 43.6 D^2, corroborating this observation. In addition, the calculated zero-phonon line (ZPL) for the HfV^- center is determined to be 1.31 eV, aiding experimental endeavors in selecting appropriate initialization wavelengths.

IV. SUMMARY

In summary, our investigation delves into the ground-state ZFS of group-III (In, Tl), group-IV (Si, Ge, Sn, Pb), group-V (Sb, Bi), and group-IVB (Ti, Zr, Hf) color centers in diamonds, employing density-functional theory and group theory analysis. Our findings elucidate that the upswing in ground-state ZFS of group-IV color centers whose atomic number stems from the collaborative interplay of heavy atom SOC and the strength of p-d orbital coupling. The reduced p-d coupling, caused by the reduced d orbital energy of impurity atom, leads to a progressive decrease in the ground-state ZFS from group-III to group-IV to group-V centers within the same period. Notably, TlV^{2-} centers exhibit a larger ground-state ZFS than PbV^- centers, despite Tl atoms having a slightly smaller atomic number than Pb atoms. The ground state of group-IVB centers is created by a robust p-p coupling between the impurity atom and divacancy, resulting in the ground-state ZFS of HfV^- center having a different representation and nearly double that experimentally observed in the largest PbV^- centers. Consequently, our study provides a more profound and comprehensive understanding of the mechanisms governing the modulation of ground-state ZFS by impurity atoms and paves the way for designing color centers in diamond with large ground-state ZFS.

ACKNOWLEDGMENTS

This paper was supported by the National Natural Science Foundation of China (Grants No. 11991060, No. 61922077, No. 12088101, No. 61927901, and No. U2230402), the National Key Research and Development Program of China (Grants No. 2020YFB1506400 and No. 2018YFB2200100), and the CAS Project for Young Scientists in Basic Research (Grant No. YSBR-026). We also acknowledge the computational support from the Beijing Computational Science Research Center.

APPENDIX: HAM REDUCTION FACTOR AND JAHN-TELLER ADIABATIC POTENTIAL ENERGY SURFACE

Here we determine the adiabatic potential energy surface (APES) for the dynamic Jahn-Teller system by manipulating ion positions. Ham and Bersuker extensively studied the $E\otimes e$ DJT system [47,49,50]. The $E\otimes e$ DJT Hamiltonian, associated with the simplest liner DJT effect, is represented as [48]

$$\hat{H} = \hbar\omega(a_x^\dagger a_x + a_y^\dagger a_y + 1) + F[(a_x + a_x^\dagger)\sigma_z + (a_y + a_y^\dagger)\sigma_x], \tag{A1}$$

where $a_x^\dagger$, $a_y^\dagger$ and a_x, a_y denote the annihilation and creation operators of the e_g (or e_u) local vibration mode, respectively. The system behaves as a two-dimensional harmonic oscillator with frequency ω, hence the $\hbar\omega$ energy is derived from a parabola fitting of the calculated APES. The component marked as F represents the electron-phonon coupling strength. The σ operator signifies the Pauli matrices of electrons. The Jahn-Teller stabilization energy (E_{JT}) denotes the energy difference resulting from symmetry distortion, and it is directly computed via total energy, typically calculated employing the HSE06 hybrid functional method. Following the relationship $E_{JT} = F^2/2\hbar\omega$, we can ascertain the F parameter. Ham has numerically solved Eq. (1) for various $\chi = E_{JT}/\hbar\omega$ values and established a fitted function as $p = \exp(-1.974 \times \chi^{0.761})$, which holds validity in the $0.1 \leqslant \chi \leqslant 3$ region, making it applicable to our calculations.

The Ham reduction factors are calculated to determine the effective spin-orbit coupling strength Δ_{GS}^{Ham}. The initial

step involves calculating the APES, as depicted in Fig. 4, by varying the ion position. For the group-IV centers, the calculated Jahn-Teller stabilization energies E_{JT} are 43.05 meV for the SiV^- center, 30.87 meV for the GeV^- center, 22.06 meV for the SnV^- center, and 15.17 meV for the PbV^- center (see Table I), exhibiting marginal variation of within 1 meV compared to a previous report [25]. Treating these DJT systems as two-dimensional harmonic oscillators, the e_g-type local vibration mode phonon frequencies ω for group-IV centers are derived by parabolic fitting to the APES. Hence, using the calculated E_{JT} and ω, the Ham reduction factor is obtained through function $p = \exp(-1.974 \times \chi^{0.761})$, where $\chi = E_{\mathrm{JT}}/\hbar\omega$. Consequently, upon implementing the Ham reduction factor correction, the resulting $\Delta_{\mathrm{GS}}^{\mathrm{Ham}}$ of 84 GHz for SiV^- centers, 230 GHz for GeV^- centers, 976 GHz for SnV^- centers, and 4445 GHz for PbV^- centers demonstrate good agreement with the experimental and calculated findings. It is important to note that all other color centers analyzed in this study underwent the same process to determine the $\Delta_{\mathrm{GS}}^{\mathrm{Ham}}$ of effective SOC.

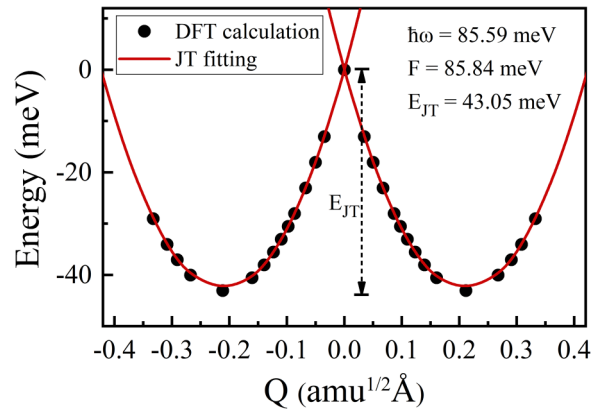

FIG. 4. The Jahn-Teller adiabatic potential energy surface illustrates the transition between D_{3d} and C_{2h} symmetry for the SiV^- center in diamond. The red line curves represent the parabolic fit to the calculated results (dots) using the density function theory. $Q = 0$ corresponds to the D_{3d} configuration. The E_{JT} denotes the total energy variation between the local minimum C_{2h} geometry and the high symmetry D_{3d} configuration within the APES.

[1] T. D. Ladd, F. Jelezko, R. Laflamme, Y. Nakamura, C. Monroe, and J. L. O'Brien, Nature (London) **464**, 45 (2010).

[2] J. J. Pla, K. Y. Tan, J. P. Dehollain, W. H. Lim, J. J. Morton, D. N. Jamieson, A. S. Dzurak, and A. Morello, Nature (London) **489**, 541 (2012).

[3] C. Bradac, W. Gao, J. Forneris, M. E. Trusheim, and I. Aharonovich, Nat. Commun. **10**, 5625 (2019).

[4] C. Qiu and H.-X. Deng, Sci. China Mater. **65**, 558 (2021).

[5] A. Gritsch, L. Weiss, J. Früh, S. Rinner, and A. Reiserer, Phys. Rev. X **12**, 041009 (2022).

[6] P. Udvarhelyi, B. Somogyi, G. Thiering, and A. Gali, Phys. Rev. Lett. **127**, 196402 (2021).

[7] G. Balasubramanian, P. Neumann, D. Twitchen, M. Markham, R. Kolesov, N. Mizuochi, J. Isoya, J. Achard, J. Beck, J. Tissler, V. Jacques, P. R. Hemmer, F. Jelezko, and J. Wrachtrup, Nat. Mater. **8**, 383 (2009).

[8] M. L. Goldman, A. Sipahigil, M. W. Doherty, N. Y. Yao, S. D. Bennett, M. Markham, D. J. Twitchen, N. B. Manson, A. Kubanek, and M. D. Lukin, Phys. Rev. Lett. **114**, 145502 (2015).

[9] S. Wehner, D. Elkouss, and R. Hanson, Science **362**, 303 (2018).

[10] H. Park, J. Lee, S. Han, S. Oh, and H. Seo, npj Quantum Inf. **8**, 95 (2022).

[11] N. Kalb, A. A. Reiserer, P. C. Humphreys, J. J. W. Bakermans, S. J. Kamerling, N. H. Nickerson, S. C. Benjamin, D. J. Twitchen, M. Markham, and R. Hanson, Science **356**, 928 (2017).

[12] C. Santori, P. E. Barclay, K. M. Fu, R. G. Beausoleil, S. Spillane, and M. Fisch, Nanotechnology **21**, 274008 (2010).

[13] D. Riedel, I. Söllner, B. J. Shields, S. Starosielec, P. Appel, E. Neu, P. Maletinsky, and R. J. Warburton, Phys. Rev. X **7**, 031040 (2017).

[14] P. Siyushev, H. Pinto, M. Voros, A. Gali, F. Jelezko, and J. Wrachtrup, Phys. Rev. Lett. **110**, 167402 (2013).

[15] H. Bernien, L. Childress, L. Robledo, M. Markham, D. Twitchen, and R. Hanson, Phys. Rev. Lett. **108**, 043604 (2012).

[16] B. Pingault, J. N. Becker, C. H. H. Schulte, C. Arend, C. Hepp, T. Godde, A. I. Tartakovskii, M. Markham, C. Becher, and M. Atatüre, Phys. Rev. Lett. **113**, 263601 (2014).

[17] M. K. Bhaskar, D. D. Sukachev, A. Sipahigil, R. E. Evans, M. J. Burek, C. T. Nguyen, L. J. Rogers, P. Siyushev, M. H. Metsch, H. Park, F. Jelezko, M. Loncar, and M. D. Lukin, Phys. Rev. Lett. **118**, 223603 (2017).

[18] T. Iwasaki, Y. Miyamoto, T. Taniguchi, P. Siyushev, M. H. Metsch, F. Jelezko, and M. Hatano, Phys. Rev. Lett. **119**, 253601 (2017).

[19] M. E. Trusheim, N. H. Wan, K. C. Chen, C. J. Ciccarino, J. Flick, R. Sundararaman, G. Malladi, E. Bersin, M. Walsh, B. Lienhard, H. Bakhru, P. Narang, and D. Englund, Phys. Rev. B **99**, 075430 (2019).

[20] C. Qiu, H.-X. Deng, S. Geng, and S.-H. Wei, Phys. Rev. B **107**, 214110 (2023).

[21] P. Siyushev, M. H. Metsch, A. Ijaz, J. M. Binder, M. K. Bhaskar, D. D. Sukachev, A. Sipahigil, R. E. Evans, C. T. Nguyen, M. D. Lukin, P. R. Hemmer, Y. N. Palyanov, I. N. Kupriyanov, Y. M. Borzdov, L. J. Rogers, and F. Jelezko, Phys. Rev. B **96**, 081201(R) (2017).

[22] K. D. Jahnke, A. Sipahigil, J. M. Binder, M. W. Doherty, M. Metsch, L. J. Rogers, N. B. Manson, M. D. Lukin, and F. Jelezko, New J. Phys. **17**, 043011 (2015).

[23] S. Ditalia Tchernij, T. Lühmann, T. Herzig, J. Küpper, A. Damin, S. Santonocito, M. Signorile, P. Traina, E. Moreva, F. Celegato, S. Pezzagna, I. P. Degiovanni, P. Olivero, M. Jakšić, J. Meijer, P. M. Genovese, and J. Forneris, ACS Photonics **5**, 4864 (2018).

[24] L. J. Rogers, K. D. Jahnke, M. H. Metsch, A. Sipahigil, J. M. Binder, T. Teraji, H. Sumiya, J. Isoya, M. D. Lukin, P. Hemmer, and F. Jelezko, Phys. Rev. Lett. **113**, 263602 (2014).

[25] G. Thiering and A. Gali, Phys. Rev. X **8**, 021063 (2018).

[26] E. Neu, D. Steinmetz, J. Riedrich-Möller, S. Gsell, M. Fischer, M. Schreck, and C. Becher, New J. Phys. **13**, 025012 (2011).
[27] C. Hepp, T. Muller, V. Waselowski, J. N. Becker, B. Pingault, H. Sternschulte, D. Steinmuller-Nethl, A. Gali, J. R. Maze, M. Atature, and C. Becher, Phys. Rev. Lett. **112**, 036405 (2014).
[28] B. Pingault, D. D. Jarausch, C. Hepp, L. Klintberg, J. N. Becker, M. Markham, C. Becher, and M. Atature, Nat. Commun. **8**, 15579 (2017).
[29] D. D. Sukachev, A. Sipahigil, C. T. Nguyen, M. K. Bhaskar, R. E. Evans, F. Jelezko, and M. D. Lukin, Phys. Rev. Lett. **119**, 223602 (2017).
[30] Y. Zhou, Z. Mu, G. Adamo, S. Bauerdick, A. Rudzinski, I. Aharonovich, and W.-b. Gao, New J. Phys. **20**, 125004 (2018).
[31] M. E. Trusheim, B. Pingault, N. H. Wan, M. Gündoğan, L. De Santis, R. Debroux, D. Gangloff, C. Purser, K. C. Chen, M. Walsh, J. J. Rose, J. N. Becker, B. Lienhard, E. Bersin, I. Paradeisanos, G. Wang, D. Lyzwa, A. R.-P. Montblanch, G. Malladi, H. Bakhru *et al.*, Phys. Rev. Lett. **124**, 023602 (2020).
[32] E. Janitz, M. K. Bhaskar, and L. Childress, Optica **7**, 1232 (2020).
[33] J. Görlitz, D. Herrmann, P. Fuchs, T. Iwasaki, T. Taniguchi, D. Rogalla, D. Hardeman, P.-O. Colard, M. Markham, M. Hatano, and C. Becher, npj Quantum Inf. **8**, 45 (2022).
[34] R. Debroux, C. P. Michaels, C. M. Purser, N. Wan, M. E. Trusheim, J. Arjona Martínez, R. A. Parker, A. M. Stramma, K. C. Chen, L. de Santis, E. M. Alexeev, A. C. Ferrari, D. Englund, D. A. Gangloff, and M. Atatüre, Phys. Rev. X **11**, 041041 (2021).
[35] P. Wang, T. Taniguchi, Y. Miyamoto, M. Hatano, and T. Iwasaki, ACS Photonics **8**, 2947 (2021).
[36] A. Gali and J. R. Maze, Phys. Rev. B **88**, 235205 (2013).
[37] G. Kresse and J. Furthmüller, Phys. Rev. B **54**, 11169 (1996).
[38] J. P. Perdew, K. Burke, and M. Ernzerhof, Phys. Rev. Lett. **77**, 3865 (1996).
[39] P. E. Blöchl, Phys. Rev. B **50**, 17953 (1994).
[40] J. Heyd, G. E. Scuseria, and M. Ernzerhof, J. Chem. Phys. **118**, 8207 (2003).
[41] A. V. Krukau, O. A. Vydrov, A. F. Izmaylov, and G. E. Scuseria, J. Chem. Phys. **125**, 224106 (2006).
[42] M. Cardona and M. L. W. Thewalt, Rev. Mod. Phys. **77**, 1173 (2005).
[43] P. Carrier and S.-H. Wei, Phys. Rev. B **70**, 035212 (2004).
[44] S.-H. Wei and A. Zunger, Appl. Phys. Lett. **72**, 2011 (1998).
[45] D. Segev and S.-H. Wei, Phys. Rev. B **68**, 165336 (2003).
[46] T. A. Abtew, Y. Y. Sun, B.-C. Shih, P. Dev, S. B. Zhang, and P. Zhang, Phys. Rev. Lett. **107**, 146403 (2011).
[47] F. S. Ham, Phys. Rev. **138**, A1727 (1965).
[48] G. Thiering and A. Gali, Phys. Rev. B **96**, 081115(R) (2017).
[49] I. Bersuker, *The Jahn-Teller Effect* (Cambridge Univesity Press, Cambridge, England, 2006).
[50] I. Bersuker and V. Polinger, *Vibronic Interactions in Molecules and Crystals*, Vol. 49 (Springer Science & Business Media, Berlin, 2012).